Applied Physics Letters PERSPECTIVE scitation.org/journal/apl

Perspective on phase-controlled currents in semiconductors driven by structured light

Cite as: Appl. Phys. Lett. **120**, 160504 (2022); doi: 10.1063/5.0089345
Submitted: 24 February 2022 · Accepted: 3 April 2022 ·
Published Online: 21 April 2022

Shawn Sederberg[1,2,a] and Paul B. Corkum[1]

AFFILIATIONS

[1]Joint Attosecond Science Laboratory, University of Ottawa and National Research Council Canada, 25 Templeton Street, Ottawa, Ontario K1N 6X1, Canada
[2]School of Engineering Science, Simon Fraser University, 8888 University Drive, Burnaby, British Columbia V5A 1S6, Canada

[a)]Author to whom correspondence should be addressed: shawn_sederberg@sfu.ca

ABSTRACT

Controlling electrons with ever-greater precision is central to both classical and quantum electronics. Since the invention of the laser, virtually every property of coherent light has been tamed, making it one of the most precise tools available to science, technology, and medicine. Coherent control involves the transduction of an exquisitely defined property of light to an electronic system, imparting coherence to an attribute of its constituent electrons. Early developments in coherent control utilized Gaussian laser beams and spatially averaged measurements. The spatial structure and orbital angular momentum of laser light provide additional degrees of freedom for steering electronic and quasiparticle excitations in condensed matter systems. In this Perspective, we first introduce the concept of coherent control in semiconductors. We then proceed to discuss the application of structured light beams to coherent control and the requirement for spatially resolved current detection. Subsequently, we present an overview of recent experiments that were performed using cylindrical vector beams and laser beams with structured phase fronts. Finally, we provide an outlook on the horizons that have emerged with these developments and future directions of interest.

INTRODUCTION

In conventional electronic circuitry, voltages applied to a semiconductor by metallic conductors serve to control both the conductivity of the semiconductor and the current flowing through it. Despite their inseparability from complementary metal-oxide-semiconductor circuits, metallic conductors are plagued by issues related to heat dissipation and resistive-capacitive latency, which have each severely limited the performance of electronic circuits for decades. More generally, currents exist when mobile electrons are present in the conduction band of a material, and when asymmetry is imparted to their momentum distribution.

More than 25 years ago, a fundamentally new form of solid-state electronic circuit was demonstrated: one that could be defined by light rather than semiconductor fabrication processes.[1] In this pioneering experiment, a pair of optical pulses was used to excite electrons from the highly symmetric ground state of a semiconductor quantum well into a conducting state. Mid-infrared pulses from a CO_2 laser (ω) at $\lambda_\omega = 10.6\,\mu$m were frequency-doubled in a nonlinear optical crystal to obtain second-harmonic pulses ($2\,\omega$) at $\lambda_{2\omega} = 5.3\,\mu$m. The energy levels of the quantum well structure complemented the laser wavelengths, such that a transition could be resonantly excited using a single photon at $\lambda_{2\omega} = 5.3\,\mu$m or two photons at $\lambda_\omega = 10.6\,\mu$m. Critically, a parity flip accompanies a single-photon transition, yielding an asymmetric electron wavefunction; parity does not flip during a two-photon transition.

When the two pulses were applied simultaneously to the quantum well, parallel quantum pathways connecting degenerate states formed an electron interferometer.[2] Balancing the transition rate of each excitation pathway resulted in strong interference between the symmetric and asymmetric wavefunctions, giving rise to optically injected charge currents flowing through the quantum well. In direct analogy to an earlier experiment performed in gas-phase rubidium atoms,[3] it was demonstrated that the relative phase between the two pulses, i.e., $\Delta\varphi_{\omega,2\omega} = 2\varphi_\omega - \varphi_{2\omega}$, could be used to control this interference, and the amplitude and direction of the injected currents. The sinusoidal dependency of the detected photocurrent as $\Delta\varphi_{\omega,2\omega}$ was incremented as shown in Fig. 1(b). This experiment brought the fundamental principle of coherent current control to a technologically relevant platform.

Shortly after this experiment, quantum interference currents in conventional semiconductors were predicted theoretically[4] and

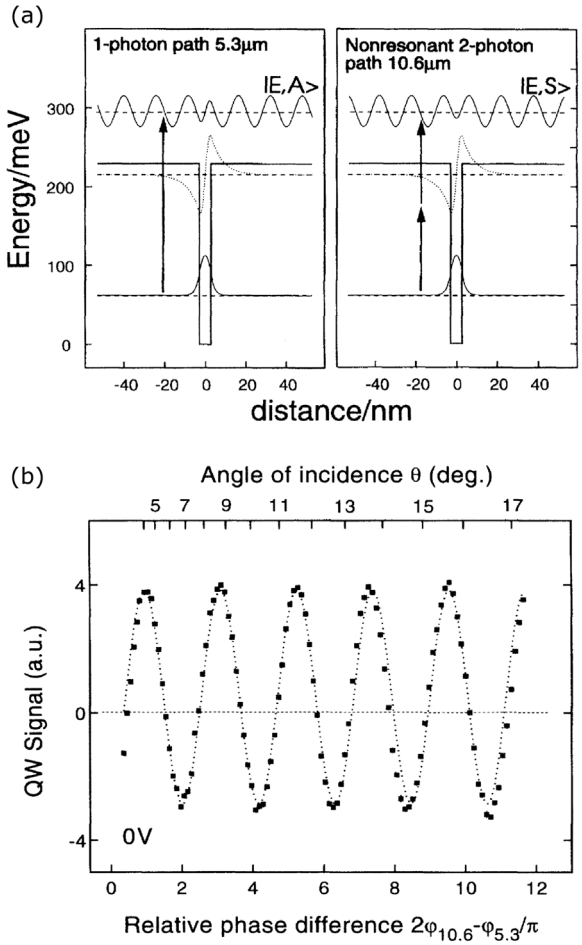

FIG. 1. Coherent control of electrical current in semiconductor quantum wells. (a) A schematic depiction of the quantum well energy structure, and the wavefunction of the excited electronic state resulting from the 1-photon path and the 2-photon path. (b) Measured current as $\Delta\varphi_{\omega,2\omega}$ is adjusted. Adapted with permission from Dupont *et al.*, Phys. Rev. Lett. **74**, 3596–3599 (1995). Copyright 1995 American Physical Society.

demonstrated experimentally.[5,6] While the direct link between atoms and quantum wells provided a clear conceptual understanding of the original experiment, the extension to conventional semiconductors was less obvious. In particular, the more intricate electronic band structure and ultrafast dephasing timescales made it unclear whether the observation of currents in these materials would be possible. Nevertheless, it was demonstrated that a similar electron interferometer could be formed using degenerate states in the valence band and conduction band of a semiconductor, depicted in Fig. 2(a). Using bichromatic femtosecond laser pulses derived from an optical parametric amplifier, currents were injected into semiconductors, including GaAs, Si, and Ge. Comprehensive experimental investigations into the scaling of the current generation process with respect to the ω and 2ω pulse intensities, and on the electrode geometry used to detect the currents provided detailed insight into the injection and detection mechanisms. These developments brought coherent control to materials and optical wavelengths that are highly relevant for modern technology.

Notably, current injection within a sub-100-femtosecond timescale and its subsequent dephasing on a few-hundred-femtosecond timescale confined the current dynamic to a sub-picosecond duration.[7] The resulting terahertz (THz)-bandwidth current modulation vastly exceeded what was possible using electrical conductors. In addition, it enabled coherent current control to be used as a source for THz radiation, where control over the current dynamic was transferred to the temporal waveform of the radiated THz pulse.[8–10] Time-domain sampling of the THz electric fields provided an alternative tool for studying the injected currents.

Although it is not directly related to the topic of this Perspective, we note that quantum interference in semiconductors can also be used to inject ballistic spin-polarized currents or to sort electron spins in momentum space, leading to spin currents in the absence of charge currents.[11,12]

Extreme temporal structuring of currents became possible when intense, few-cycle, carrier-envelope-phase (CEP) stabilized pulses were applied to dielectrics with a large bandgap energy.[13–17] When operating in the strong-field regime, transitions between the valence band and conduction band become temporally confined to bursts that are slightly delayed with respect to the electric field extrema of the laser pulse. The CEP was used to control both the time-dependent transition rate and the final momentum imparted to the conduction band electrons. From an alternative perspective, a few-cycle laser pulse contains sufficiently broad spectral content to drive two or more multiphoton transition processes simultaneously, e.g., four- and five-photon absorption. Just as for $\omega - 2\omega$ fields, parallel multi-photon channels resemble an electron interferometer. Reducing the pulse duration to a single optical cycle enabled currents to be controlled on timescales of several hundred attoseconds, demonstrating the potential for optoelectronic circuitry operating at petahertz bandwidths. We note that similar measurements have been performed in graphene[18–22] and in nanostructures.[23–25]

Optical excitation of transient currents has three important consequences: optoelectronic circuitry, control of magnetic fields in the near field of the excited currents, and THz electromagnetic radiation. Currents controlled by conventional Gaussian laser beams can be viewed as a single circuit element, where the excited currents are spatially unidirectional [Figs. 2(b) and 2(c)]. Although unidirectional currents served to illustrate the concept of coherent control in condensed matter systems, the current structure did not yet resemble an electronic circuit.

Modern optical technology enables flexible control over the spatial structure and orbital angular momentum (OAM) of light.[30–36] Applying spatially structured beams to coherent control introduces the possibility to excite intricate current circuits. For example, a cylindrical vector beam can be used to excite a current arrangement that bears similarity to the electric field configuration of the mode, as shown in Figs. 2(d) and 2(e). Alternatively, the phase structure can be applied to the ω and 2ω beams, either in a static manner using a phase plate or in a programmable manner using a spatial light modulator (SLM). When phase-structured ω and 2ω beams are applied to coherent control, their phase fronts in the excitation plane define a spatially varying relative phase, i.e., $\Delta\varphi_{\omega,2\omega}(x,y)$. This establishes control over numerous current elements in the target system, as depicted in

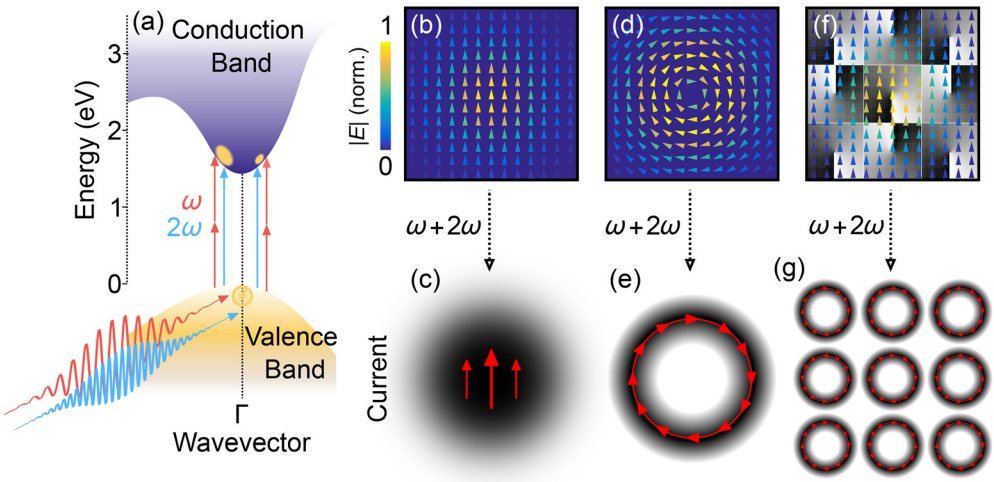

FIG. 2. Coherent control in semiconductors—from Gaussian beams to structured light. (a) Schematic depiction of coherent control of momentum asymmetry of the conduction band population of GaAs, resulting from quantum interference between single- and two-photon transitions. (b) Spatio-vectorial electric field arrangement of the lowest-order Gaussian laser mode. (c) Currents excited by ω and 2ω pulses with the mode shown in (b) will all flow in the same direction. (d) Spatio-vectorial electric field arrangement of a cylindrical vector beam with azimuthal polarization. (e) Performing coherent control with azimuthally polarized ω and 2ω beams will result in current arrangements resembling the driving electric fields—in this case, a ring current. (f) The sensitivity of coherently controlled currents to $\Delta\varphi_{\omega,2\omega}$ motivates the use of light whose phase fronts have been structured by a spatial light modulator (SLM) to programmable control more general current arrangements. (g) Applying the SLM pattern shown in (f) to coherent control will produce an array of ring currents. Adapted with permission from Sederberg *et al.*, Nat. Photonics **14**, 680–685 (2020). Copyright 2020 Nature Publishing Group.

Figs. 2(f) and 2(g). Notably, alternative schemes for optically controlling currents, including photoconductive switches,[26,27] the photovoltaic effect,[28,29] and shift currents, depend strongly on the electrode geometry or crystal orientation of the sample, restricting the flexibility of the current patterns that can be excited. Therefore, coherent control provides a unique opportunity to drive intricate dynamic current arrangements and to spatially structure magnetic fields and THz radiation.

The Biot–Savart law is a magneto-static expression that relates the spatial arrangement of magnetic fields to current elements

$$\mathbf{B}(\mathbf{r}) = \frac{\mu_0}{4\pi}\int\int\int \frac{(\mathbf{J}dV)\times\mathbf{r}'}{|\mathbf{r}'|^3},$$

where μ_0 is the permeability of free space, $\mathbf{J}(\mathbf{r})$ is the current density, and $\mathbf{r}'$ is the position vector between a current density element and the point in space under evaluation. Extending this to dynamic currents requires the formalism of retarded potentials

$$\mathbf{A}(\mathbf{r},t) = \frac{\mu_0}{4\pi}\int \frac{\mathbf{J}(\mathbf{r}',t_r)}{|\mathbf{r}-\mathbf{r}'|}\mathrm{d}^3\mathbf{r}',$$
$$t_r = \frac{|\boldsymbol{r}-\boldsymbol{r}'|}{c},$$
$$\mathbf{B} = \nabla\times\mathbf{A}.$$

Here, $\mathbf{A}(\mathbf{r},t)$ is the magnetic potential, t_r is the finite time required for information about a current to travel from the source position to the observation position, c is the speed of light, and $\mathbf{B}$ is the magnetic field. In either case, increasing the number of current elements provides additional degrees of freedom for introducing intricate spatial structure to magnetic fields.

As each dynamic current element rises and decays, it contributes electric dipole THz radiation to its surrounding volume. When many current elements are coordinated, it becomes possible to excite well-defined sub-cycle THz structured light modes that propagate through space. Therefore, coherent control provides a unique opportunity to generate ultrabroadband and reconfigurable structured light beams. In this regard, the collection of current elements can be viewed as an active, reconfigurable metasurface.

SPATIO-VECTORIAL SEMICONDUCTOR CURRENT MAPPING

A clear demonstration that structure can be transferred from light to currents requires that the spatio-vectorial arrangement of the currents be directly measured.[37–39] In conventional coherent control measurements, it is sufficient to integrate two large electrodes onto the active medium. When connected to an electronic amplifier, these electrodes enable collection and detection of a time-integrated current signal that is related to the coherently injected current. The intricate spatio-vectorial arrangement of currents excited by structured light beams necessitates a more advanced detection scheme. As depicted in Fig. 3(a), when a simple two-electrode structure is used, currents can be excited in different directions at each position within the semiconductor gap, leading to spatial averaging of the detected currents, and a loss of information about the spatio-vectorial current arrangement.

To overcome this, an optical mask is introduced immediately before the detector, as shown in Fig. 3(b). In combination with the underlying electrodes, this mask limits the spatial extent of light incident on the semiconductor to a small, square pixel, wherein the current direction is essentially uniform. The first implementation of our detector provided a pixel with $25\times25\ \mu\mathrm{m}^2$ dimensions. To demonstrate control over several hundred current pixels, we chose to work with loosely focused laser beams with a focal spot diameter on the order of 300–500 μm.

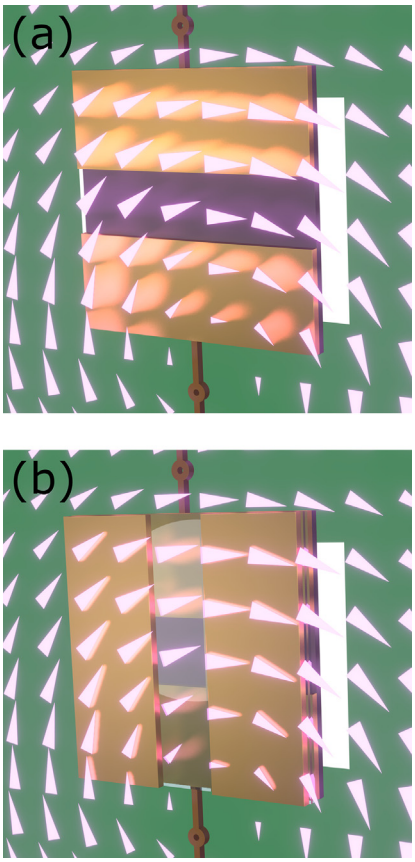

FIG. 3. A detector for spatio-vectorial mapping of semiconductor currents. (a) Schematic of a LT-GaAs substrate with two large electrodes separated by a gap. Notably, currents injected into the semiconductor may not all flow in the same direction, and spatial averaging can severely influence the measurement. (b) Positioning a dielectric substrate with a metallic mask in front of the detector limits the spatial extent of light that enters the semiconductor, such that the injected currents are unidirectional. Adapted with permission from Sederberg *et al.*, Nat. Photonics **14**, 680–685 (2020). Copyright 2020 Nature Publishing Group.

Positioning the detection pixel at different coordinates within the beam enables the local current to be sampled. To obtain a complete spatio-vectorial mapping of the excited currents, the detector is raster scanned across the plane irradiated by the laser beams. Due to the high directional sensitivity of this detector, performing such a scan with the detector positioned in one orientation provides one vectorial component of the currents (e.g., the x-component). Rotating the detector by 90° and repeating the scan then provide the orthogonal current component. Superimposing these two scans provides a complete visualization of the transverse spatio-vectorial current arrangement that would be excited in a bulk semiconductor.

VECTORIZED OPTOELECTRONIC CONTROL

Cylindrical vector beams (CVBs) offer a simple alternative to conventional Gaussian laser modes. One example of a CVB is shown Fig. 2(d): an azimuthally polarized CVB. Rotating the local electric fields by 90° produces a radially polarized CVB, where the electric fields point inward or outward from the center of the beam. Cylindrical vector beams can be generated routinely by transmitting a Gaussian mode through a pixelated waveplate optic, such as a q-plate or s-plate. Due to the electric field structure of CVBs, nonlinear optical interactions in a crystal will depend on the local electric field direction relative to the crystal orientation. Therefore, it is not trivial to frequency-double the fundamental pulse to obtain a second-harmonic pulse with the same mode. In combination with the limited bandwidth of q-plates and s-plates, it is necessary to independently convert the ω and 2ω beams to CVBs using a two-color interferometer.

Due to the microscopic origins of coherent control, when bi-chromatic CVBs are introduced to a semiconductor, the spatio-vectorial arrangement of the CVB is transferred to a spatio-vectorial current arrangement. The current arrangement measured from an azimuthally polarized CVB is displayed in Fig. 4(a), where a ring current has been excited. A snapshot of the calculated magnetic field that accompanies the measured current elements is shown in Fig. 4(b). This longitudinal, THz-bandwidth magnetic field embodies a source for ultrafast, spatially isolated magnetic fields. Applying radially polarized CVBs to coherent control produces a radial current arrangement, depicted in Fig. 4(c). Although this configuration will not produce a useful magnetic field, it can be used to control charge density dynamics in the semiconductor [Fig. 4(d)].

Subsequent adjustment of $\Delta\varphi_{\omega,2\omega}$ controls the amplitude and sign of the current excited by each "pixel" of the beam. In the case of azimuthally polarized CVBs, this controls whether the resulting currents flow clockwise or counterclockwise. For radially polarized CVBs, the current can be made to flow outward or inward.

USING CIRCULARLY POLARIZED LIGHT FOR RECONFIGURABILITY

An additional degree of control is introduced when one of the beams is circularly polarized. The x- and y-electric fields of circularly polarized light permit control of the x- and y-momentum components of the conduction band population. We consider the case where the 2ω beam has radial polarization and the ω beam has circular polarization and carries one unit of OAM, $\hbar$. In this case, the role of the OAM is to synchronize the relative polarization between the ω and 2ω beams at each azimuthal coordinate. Adjustment of $\Delta\varphi_{\omega,2\omega}$ rotates the local current direction excited by each pixel of the beams. In general, the resulting current arrangement can be written as a superposition between radial and azimuthal current configurations

$$|i\rangle = c_a|a\rangle + c_r|r\rangle,$$

where $|i\rangle$ is the spatial current arrangement, $|a\rangle$ is an azimuthal current arrangement, c_a is a coefficient representing the azimuthal contribution to $|i\rangle$, $|r\rangle$ is a radial current arrangement, and c_r represents the radial contribution to $|i\rangle$.

Such control is verified by spatially scanning the y-component of the current as $\Delta\varphi_{\omega,2\omega}$ is adjusted, which is displayed in Fig. 5. Two lobes are observed in each spatial scan: one containing positive current and the other negative current. These two lobes rotate as $\Delta\varphi_{\omega,2\omega}$ is adjusted, and for $\Delta\varphi_{\omega,2\omega} = 119.2°$, the scan resembles the y-component of a purely azimuthal current, whereas for $\Delta\varphi_{\omega,2\omega} = 208.6°$, the measurements depict the y-component of a purely radial current. Clearly, full control over $|i\rangle$ is demonstrated.

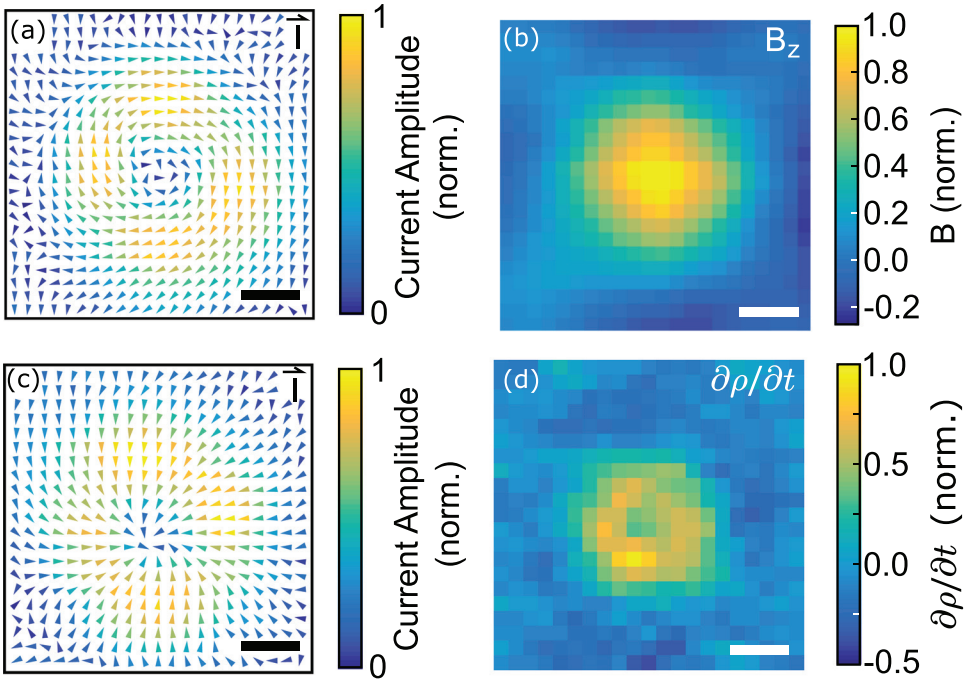

FIG. 4. Coherent control using cylindrical vector beams. (a) Spatio-vectorial current arrangement measured when the ω and 2ω pulses both have azimuthal polarization. Notably the current arrangement resembles a ring currents. (b) A snapshot of the dynamic magnetic field distribution inferred from the current arrangement in (a). (c) Spatio-vectorial current arrangement measured when the ω and 2ω pulses both have radial polarization. (d) Charge density dynamic calculated from the current arrangement in (c). Scale bars, 100 μm. Adapted with permission from Sederberg *et al.*, Nat. Photonics **14**, 680–685 (2020). Copyright 2020 Nature Publishing Group.

RECONFIGURABLE OPTOELECTRONIC CIRCUITS USING CIRCULARLY POLARIZED LIGHT

The degree of reconfigurability can be vastly expanded when greater spatial structure is imparted to the driving light fields. An SLM can be used to introduce pixelated structure to the phase front of an optical beam and can, therefore, be used to control $\Delta\varphi_{\omega,2\omega}$ as a function of the spatial coordinate, i.e., $\Delta\varphi_{\omega,2\omega}(x,y)$. In particular, when the phase fronts of one beam are sculpted by a SLM and the other beam has circular polarization, it becomes possible to transduce $\Delta\varphi_{\omega,2\omega}(x,y)$ into the spatially dependent current direction. Modern SLMs enable programmable control over megapixel arrays of liquid crystal phase retarding elements, making it possible to program very complicated electronic circuits.

As a proof-of-principle, we use a circularly polarized ω beam and a linearly polarized 2ω beam that has been reflected from an SLM. Using this scheme, we demonstrate independent and programmable control over the direction of several hundred current elements. In the interest of using the currents for optoelectronic information

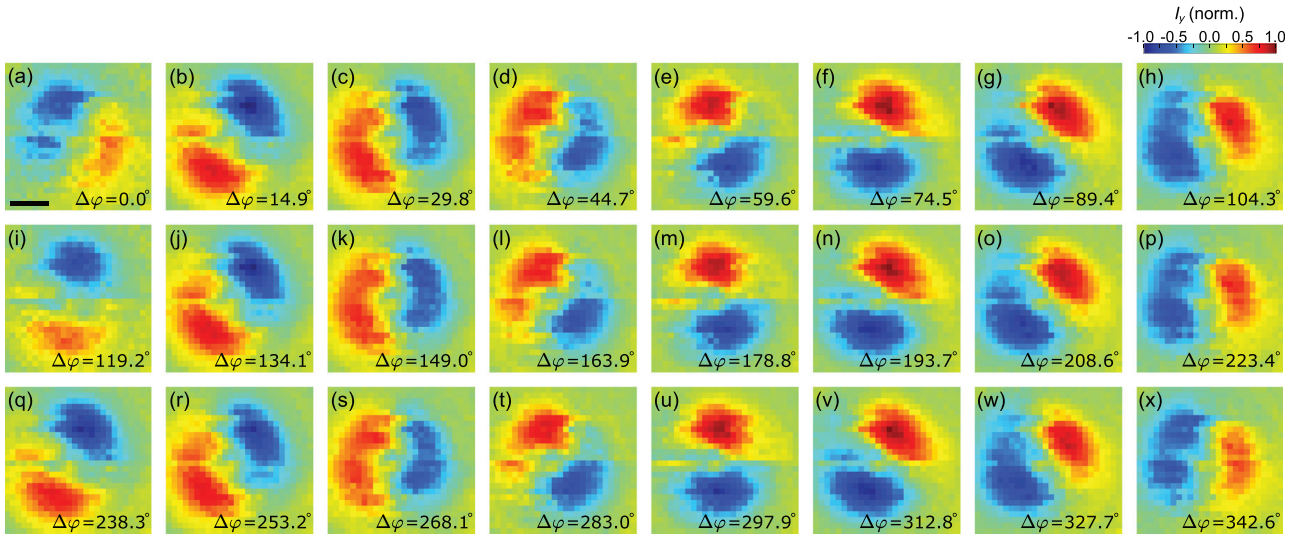

FIG. 5. Reconfiguring current arrangements using circular polarization. (a)–(x) depict the spatial arrangement of the *y*-component of the detected current as $\Delta\varphi_{\omega,2\omega}$ is incremented in 14.9° steps. Scale bar, 100 μm. Adapted with permission from Sederberg *et al.*, Nat. Photonics **14**, 680–685 (2020). Copyright 2020 Nature Publishing Group.

processing, we excite wire-like current features. Although we do not demonstrate optoelectronic signal transfer in real electronic circuits, we envisage that wire-like features could be introduced to existing electronic circuitry to act as interconnects or as a security feature. An example of an imaginary optoelectronic circuit is depicted in Fig. 6(a) and the wire-like features that are excited are shown in Fig. 6(b). We note that the SLM used in this measurement could not modulate the amplitude of the optical beam, making it challenging to completely suppress currents in the regions outside of the wire-like feature.

We also explore the possibility to use programmable current elements to spatially structure magnetic fields. Two examples are shown in Fig. 7. Figure 7(a) depicts a square current arrangement that is controlled using the SLM. The calculated magnetic field exhibits square structure [Fig. 7(b)]. Reconfiguring the SLM pattern enables considerable diversity in the current arrangements that are excited, such as the one displayed in Fig. 7(c). This current arrangement has been optimized to excite a "bull's eye" magnetic field [Fig. 7(d)].

To demonstrate extreme spatial structuring of magnetic fields, we excite 3×3 arrays of ring currents, which generate 3×3 magnetic field lattices. An exemplary current measurement where the ring currents all flow clockwise is shown in Fig. 7(a), which would produce the magnetic field lattice displayed in Fig. 7(b). Adjusting the SLM pattern enables the amplitude and direction of the magnetic field at each lattice site to be controlled. A modified current arrangement, where a radial current has been introduced to the center lattice site [Fig. 7(c)], suppresses the magnetic field at this site [Fig. 7(d)].

Although we have not yet characterized the temporal structure of the magnetic fields, we note the possibility to simultaneously sculpt the spatial and temporal structure of magnetic fields within the plane of the semiconductor. Numerical examples of current patterns resembling concentric rings are shown in the left-hand panels of Fig. 8. Calculating the time-varying magnetic field at the center of the rings produces the plots shown in the corresponding right-hand panels. Periodicity in the concentric ring currents translates into the frequency and waveform of the local magnetic field. Control over the spatial current arrangements, therefore, enables tuning of the magnetic field spectrum for resonant excitation of, e.g., magnons.[40]

OUTLOOK ON STRUCTURED COHERENT CONTROL

As outlined earlier, fine control of transient currents using structured light has three important consequences: optoelectronic circuitry,

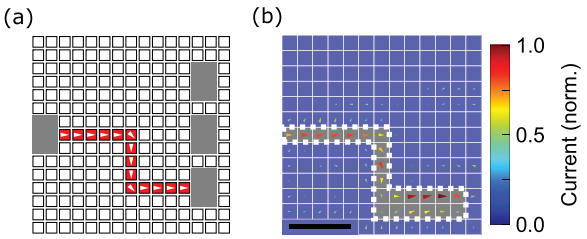

FIG. 6. Reconfigurable optoelectronic interconnects. (a) Circuit schematic of one electrode on the left-hand side that can be connected to one of three electrodes on the right-hand side. (b) Spatio-vectorial current arrangement demonstrating programmable control of currents flowing into the bottom-most electrode on the right-hand side. Scale bar, 100 μm. Adapted with permission from Jana *et al.*, Nat. Photonics **15**, 622–626 (2021). Copyright 2021 Nature Publishing Group.

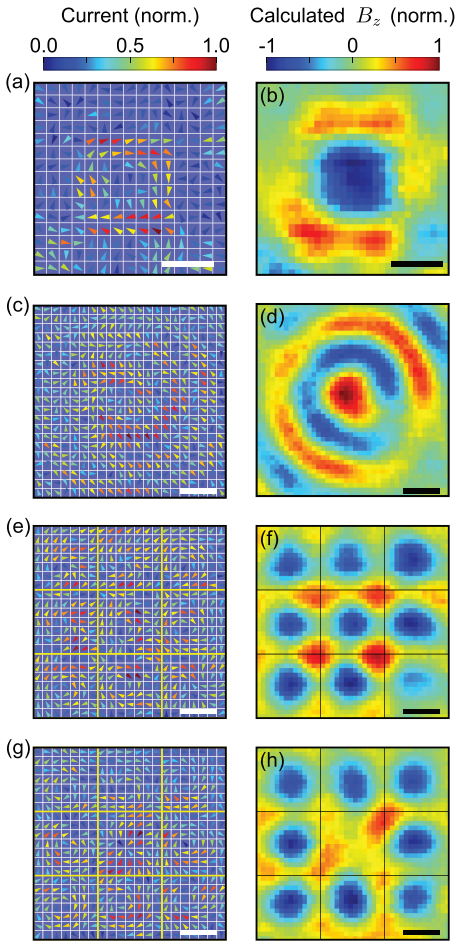

FIG. 7. Programmable current arrangements for spatially structured magnetic fields. (a) and (b) A square ring current and a snapshot of its corresponding magnetic field, respectively. (c) and (d) A spiral ring current and a snapshot of the resulting bull's eye magnetic field arrangement, respectively. (e) and (f) A lattice of ring currents circulating clockwise and the lattice of magnetic fields, respectively. (g) A lattice of ring currents similar to that shown in (e), but with a radial current introduced to the central lattice site. (h) The corresponding magnetic fields. Notably, the radial current does not produce a magnetic field. Scale bars, 100 μm. Adapted with permission from Jana *et al.*, Nat. Photonics **15**, 622–626 (2021). Copyright 2021 Nature Publishing Group.

spatially structured magnetic impulses, and structured, sub-cycle THz electromagnetic pulses.

Controlling and measuring currents on smaller and smaller length scales approaching the light wave diffraction limit would enable high-density optoelectronic circuits to be dynamically excited. Recently, we have extended the concepts presented here to achieve control and measurement of currents on 6-μm length scales.[39] Using megapixel SLMs to control intricate, micrometer-scale optoelectronic circuits in semiconductors introduce exciting technological capabilities. In particular, reconfigurability, the elimination of fabricated structures, and THz-bandwidth current modulation are each unique features that surpass those offered by conventional circuitry platforms. Using the intrinsic or orbital angular momentum of light, it also becomes possible

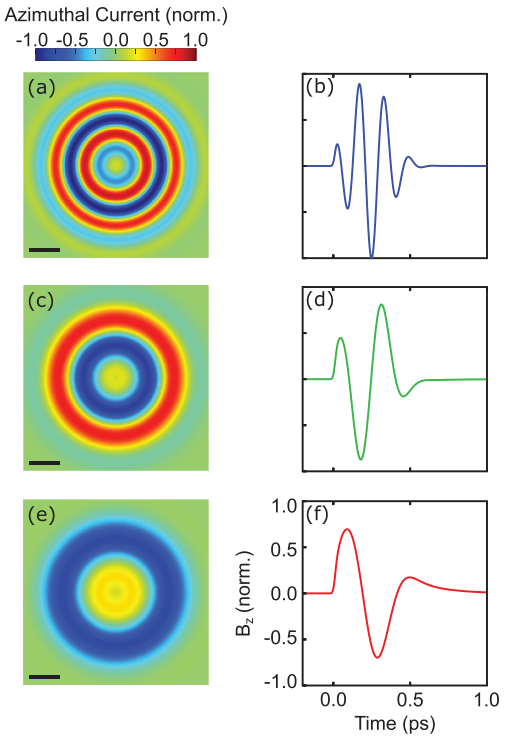

FIG. 8. Transferring spatial structure of currents to the temporal structure of magnetic fields. (a), (c), and (e) Current arrangements consisting of concentric ring currents flowing in alternating directions. The radial extent of the currents is the same for each figure, but the width of the current rings (i.e., the period) increases from (a) to (e). (b), (d), and (f) The time-dependent magnetic field calculated at the center of the current rings in (a), (c), and (e), respectively. Scale bars, 50 μm.

to control spin currents with similar structure, extending each of the concepts presented here toward spintronic applications.

Fine control of magnetic fields is a direct outcome of coherently controlled currents. The impulsive character of the currents provides an impulsive magnetic field source. The reliance of conventional electromagnets on electrical conductors and superconductors limits the modulation bandwidth of magnetic fields generated using the available sources. Using femtosecond laser pulses to excite magnetic fields that are both strong and brief will facilitate exploration of experimental regimes that were not previously accessible, including the breakdown of conventional magnetization dynamics, nonlinear spin manipulation, and phase transition dynamics.[41–48]

Notably, magnetic materials and devices can be fabricated directly onto the semiconductor where ring currents are excited, enabling the magnetic fields to be used directly where they are generated. By fabricating structures composed of magnetic materials onto the semiconductor, and exciting ring currents around these structures, it will be possible to introduce enhanced and highly localized magnetic fields to the sample.

While semiconductors are a technologically relevant platform for generating magnetic fields, we note that similar current excitations in gas-phase media will be required to excite tesla-scale magnetic fields.[49] Large magnetic fields require high current densities, and current density scaling in solid-state platforms is ultimately limited by saturation and damage mechanisms. Based on two independent estimates of the maximum magnetic field, one based on experimental THz electric fields generated from GaAs photoconductive switches and the other from simple magneto-static calculations, we envisage magnetic field scaling up to approximately 50 mT in semiconductors.[50] Gas-phase targets have two important advantages: They are continuously replenished, and they are characterized by a high ionization potential. This enables very intense optical fields to be applied to the target before ionization occurs, and they subsequently accelerate the photoelectrons to high kinetic energies. The potential for generating magnetic fields on the order of 8 T has been demonstrated numerically,[51] and we anticipate that alternative excitation schemes could enable scaling up to 100 T. Scaling optically excited magnetic fields to amplitudes that exceed those produced in electromagnets may one day enable exploration of exciting phenomena in quantum systems.

Controlling magnetic fields at the nanoscale enables excitation of quasiparticles, such as magnetic skyrmions. While the spatial resolution of the excited currents is constrained by the light wave diffraction limit, we envisage two routes to nanoscale magnetic fields. The first is to use extreme ultraviolet light for one of the pulses used to drive coherent control. The second is to combine the principles of coherent control with nanostructured thin films. It has recently been demonstrated that carefully arranged nanoscale slits in metallic films enable the excitation of plasmonic skyrmions and topological quasiparticles.[52–56] Ultimately, it is desirable to not only excite quasiparticles, but to steer them. Structured coherent control at the nanoscale will broaden the scope of excitations and quasiparticles that can be manipulated.[57,58]

Over the last 25 years, the scope of control parameters, materials, and detection schemes used in coherent control has expanded considerably. Laser and optical technology now make shorter, more intense optical pulses available from the deep ultraviolet to the THz spectral region,[59–64] with vast control over their spatial and temporal character. With the development of new materials comes the opportunity to investigate and utilize new quantum interference phenomena and to control topological excitations. Coherent control has also been explored in a broader array of light-matter interaction regimes,[65] including dressed states,[66] metals,[67,68] and systems exhibiting strong light-matter coupling. Finally, advanced tools for measuring coherent electronic phenomena have matured, namely, photoemission spectroscopy,[69] angular-resolved photoemission spectroscopy,[70] transient absorption spectroscopy,[71] high-harmonic spectroscopy,[72] scanning probe microscopy,[73] and electron diffraction techniques.[47]

In this Perspective, we bring many of the concepts that originally motivated coherent control in solid-state platforms into reality. While we have demonstrated the principles of control and measurement using structured light, we have only begun to explore how it can be useful for science and technology. Increasing the spatial resolution of currents, combining structured light with nanostructured materials, controlling currents with shorter optical pulses, and scaling the amplitude of currents will each enable exciting possibilities in magnetic field spectroscopy and condensed matter physics.

ACKNOWLEDGMENTS

The authors gratefully acknowledge funding from the United States Defense Advanced Research Projects Agency (Topological

Excitations in Electronics (TEE), Agreement No. D18AC00011), the United States Army Research Office (Award No. W911NF-19-1-0211), the Natural Sciences and Engineering Research Council of Canada Discovery Grant program, and the Canada Research Chairs program. The authors emphasize that the results presented in this manuscript summarize the experimental efforts of Kamalesh Jana, Yonghao Mi, Søren Møller, Fanqi Kong, Chunmei Zhang, Katherine Herperger, and Emmanuel Okocha. We thank each of them for the fruitful collaboration and for many stimulating discussions.

AUTHOR DECLARATIONS

Conflict of Interest

The authors declare no conflicts of interest.

DATA AVAILABILITY

The data that support the findings of this study are available from the corresponding author upon reasonable request.

REFERENCES

[1]E. Dupont, P. B. Corkum, H. C. Liu, M. Buchanan, and Z. R. Wasilewksi, "Phase-controlled currents in semiconductors," Phys. Rev. Lett. **74**, 3596–3599 (1995).
[2]M. Shapiro and P. Brumer, *Quantum Control of Molecular Processes* (John Wiley & Sons, 2012).
[3]Y. Y. Yin, C. Chen, and D. S. Elliot, "Asymmetric photoelectron angular distributions from interfering photoionization processes," Phys. Rev. Lett. **69**, 2353–2356 (1992).
[4]R. Atanasov, A. Haché, J. L. P. Hughes, H. M. van Driel, and J. E. Sipe, "Coherent control of photocurrent injection in bulk semiconductors," Phys. Rev. Lett. **76**, 1703–1706 (1996).
[5]A. Haché, Y. Kostoulas, R. Atanasov, J. L. P. Hughes, J. E. Sipe, and H. M. van Driel, "Observation of coherently controlled photocurrent in unbiased, bulk GaAs," Phys. Rev. Lett. **78**, 306–309 (1997).
[6]A. Haché, J. E. Sipe, and H. M. van Driel, "Quantum interference control of electrical currents in GaAs," IEEE J. Quantum Electron. **34**, 1144–1154 (1998).
[7]H. Zhao, E. J. Loren, A. L. Smirl, and H. M. van Driel, "Dynamics of charge currents ballistically injected in GaAs by quantum interference," J. Appl. Phys. **103**, 053510 (2008).
[8]D. Côté, J. M. Fraser, M. DeCamp, P. H. Bucksbaum, and H. M. van Driel, "THz emission from coherently controlled photocurrents in GaAs," Appl. Phys. Lett. **75**, 3959–3961 (1999).
[9]L. Costa, M. Betz, M. Spasenovic, A. D. Bristow, and H. M. van Driel, "All-optical injection of ballistic electrical currents in unbiased silicon," Nat. Phys. **3**, 632–635 (2007).
[10]M. Spasenovic, M. Betz, L. Costa, and H. M. van Driel, "All-optical injection of electrical currents in centrosymmetric semiconductors," Phys. Rev. B **77**, 085201 (2008).
[11]M. J. Stevens, A. L. Smirl, R. D. R. Bhat, A. Najmaei, J. E. Sipe, and H. M. van Driel, "Quantum interference control of ballistic spin currents in semiconductors," Phys. Rev. Lett. **90**, 136603 (2003).
[12]J. Hübner, W. W. Rühle, M. Klude, D. Hommel, R. D. R. Bhat, J. E. Sipe, and H. M. van Driel, "Direct observation of optically injected spin-polarized currents in semiconductors," Phys. Rev. Lett. **90**, 216601 (2003).
[13]A. Schiffrin, T. Paasch-Colberg, N. Karpowicz, V. Apalkov, D. Gerster, S. Mühlbrandt, M. Korbman, J. Reichert, M. Schultze, S. Holzner, J. V. Barth, R. Kienberger, R. Ernstorfer, V. S. Yakovlev, M. I. Stockman, and F. Krausz, "Optical-field-induced currents in dielectrics," Nature **493**, 70–74 (2013).
[14]T. Paasch-Colberg, A. Schiffrin, N. Karpowicz, S. Kruchinin, Ö. Saglam, S. Keiber, O. Razskazovskaya, S. Mühlbrandt, A. Alnaser, M. Kübel, V. Apalkov, D. Gerster, J. Reichert, T. Wittmann, J. V. Barth, M. I. Stockman, R. Ernstorfer, V. S. Yakovlev, R. Kienberger, and F. Krausz, "Solid-state light-phase detector," Nat. Photonics **8**, 214–218 (2014).
[15]T. Paasch-Colberg, S. Yu Kruchinin, Ö. Saglam, S. Kapser, S. Cabrini, S. Mühlbrandt, J. Reichert, J. V. Barth, R. Ernstorfer, R. Kienberger, V. S. Yakovlev, N. Karpowicz, and A. Schiffrin, "Sub-cycle optical control of current in a semiconductor: From the multiphoton to the tunnelling regime," Optica **3**, 1358–1361 (2016).
[16]S. Sederberg, D. Zimin, S. Keiber, F. Siegrist, M. S. Wismer, V. S. Yakovlev, I. Floss, C. Lemell, J. Burgdörfer, M. Schultze, F. Krausz, and N. Karpowicz, "Attosecond optoelectronic field measurement in solids," Nat. Commun. **11**, 430 (2020).
[17]V. Hanus, V. Csajbok, Z. Papa, J. Budai, Z. Marton, G. Z. Kiss, P. Sandor, P. Paul, A. Szeghalmi, Z. Wang, B. Bergues, M. F. Kling, G. Molnar, J. Volk, and P. Dombi, "Light-field-driven current control in solids with pJ-level laser pulses at 80 MHz repetition rate," Optica **8**, 570–576 (2021).
[18]T. Higuchi, C. Heide, K. Ullmann, H. B. Weber, and P. Hommelhoff, "Light-field-driven currents in graphene," Nature **550**, 224–228 (2017).
[19]C. Heide, T. Higuchi, H. B. Weber, and P. Hommelhoff, "Coherent electron trajectory control in graphene," Phys. Rev. Lett. **121**, 207401 (2018).
[20]T. Boolakee, C. Heide, F. Wagner, C. Ott, M. Schlecht, J. Ristein, H. B. Weber, and P. Hommelhoff, "Length-dependence of light-induced currents in graphene," J. Phys. B **53**, 154001 (2020).
[21]C. Heide, T. Boolakee, T. Eckstein, and P. Hommelhoff, "Optical current generation in graphene: CEP control vs $\omega + 2\omega$ control," Nanophotonics **10**, 3701–3707 (2021).
[22]C. Heide, T. Eckstein, T. Boolakee, C. Gerner, H. B. Weber, I. Franco, and P. Hommelhoff, "Electronic coherence and coherent dephasing in the optical control of electrons in graphene," Nano Lett. **21**, 9403–9409 (2021).
[23]T. Rybka, M. Ludwig, M. F. Schmalz, V. Knittel, D. Brida, and A. Leitenstorfer, "Sub-cycle optical phase control of nanotunnelling in the single-electron regime," Nat. Photonics **10**, 667–670 (2016).
[24]M. Ludwig, G. Aguirregabiria, F. Ritzkowsky, T. Rybka, D. C. Marinica, J. Aizpurua, A. G. Borisov, A. Leitenstorfer, and D. Brida, "Sub-femtosecond electron transport in a nanoscale gap," Nat. Phys. **16**, 341–345 (2020).
[25]M. R. Bionta, F. Ritzkowsky, M. Turchetti, Y. Yang, D. C. Mor, W. P. Putnam, F. X. Kärtner, K. K. Berggren, and P. D. Keathley, "On-chip sampling of optical fields with attosecond resolution," Nat. Photonics **15**, 456–460 (2021).
[26]D. H. Auston, "Picosecond optoelectronic switching and gating in silicon," Appl. Phys. Lett. **26**, 101–103 (1975).
[27]D. H. Auston, "Ultrafast optoelectronics," Top. Appl. Phys. **60**, 183–233 (1988).
[28]V. I. Belinicher and B. I. Sturman, "The photogalvanic effect in media lacking a center of symmetry," Sov. Phys. Usp. **23**, 199–223 (1980).
[29]T. Choi, S. Lee, Y. J. Choi, V. Kiryukhin, and S.-W. Cheong, "Switchable ferroelectric diode and photovoltaic effect in $BiFeO_3$," Science **324**, 63–66 (2009).
[30]Q. Zhan, "Cylindrical vector beams: From mathematical concepts to applications," Adv. Opt. Photonics **1**, 1–57 (2009).
[31]N. Yu and F. Capasso, "Flat optics with designer metasurface," Nat. Mater. **13**, 139–150 (2014).
[32]A. Forbes, A. Dudley, and M. McLaren, "Creation and detection of optical modes with spatial light modulators," Adv. Opt. Photonics **8**, 200–227 (2016).
[33]D. Naidoo, F. S. Roux, A. Dudley *et al.*, "Controlled generation of higher-order Poincaré sphere beams from a laser," Nat. Photonics **10**, 327–332 (2016).
[34]H. Rubinsztein-Dunlop, A. Forbes, M. V. Berry *et al.*, "Roadmap on structured light," J. Opt. **19**, 013001 (2017).
[35]C. Rosales-Guzman, B. Ndagano, and A. Forbes, "A review of complex vector light fields and their applications," J. Opt. **20**, 123001 (2018).
[36]A. Forbes, M. de Oliveira, and M. R. Dennis, "Structured light," Nat. Photonics **15**, 253–262 (2021).
[37]S. Sederberg, F. Kong, F. Hufnagel *et al.*, "Vectorized optoelectronic control and metrology in a semiconductor," Nat. Photonics **14**, 680–685 (2020).
[38]K. Jana, K. R. Herperger, F. Kong *et al.*, "Reconfigurable electronic circuits for magnetic fields controlled by structured light," Nat. Photonics **15**, 622–626 (2021).
[39]K. Jana, E. Okocha, S. H. Møller *et al.*, "Reconfigurable terahertz metasurfaces coherently controlled by wavelength-scale-structure light," Nanophotonics **11**, 787 (2022).

[40]A. Barman, G. Gubbiotti, S. Ladak *et al.*, "The 2021 magnonics roadmap," J. Phys. **33**, 413001 (2021).
[41]J.-Y. Bigot, M. Vomir, and E. Beaurepaire, "Coherent ultrafast magnetism induced by femtosecond laser pulses," Nat. Phys. **5**, 515–520 (2009).
[42]J. Walowski and M. Münzenberg, "Ultrafast magnetism and THz spintronics," J. Appl. Phys. **120**, 140901 (2016).
[43]S. Baierl, M. Hohenleutner, T. Kampfrath *et al.*, "Nonlinear spin control by terahertz-driven anisotropy fields," Nat. Photonics **10**, 715–718 (2016).
[44]F. Siegrist, J. A. Gessner, M. Ossiander *et al.*, "Light-wave dynamic control of magnetism," Nature **571**, 240–244 (2019).
[45]C. Boeglin, E. Beaurepaire, V. Halté *et al.*, "Distringuishing the ultrafast dynamics of spin and orbital moments in solids," Nature **465**, 458–461 (2010).
[46]A. Kirilyuk, A. Kimel, and T. Rasing, "Ultrafast optical manipulation of magnetic order," Rev. Mod. Phys. **82**, 2731–2784 (2010).
[47]S. R. Tauchert, M. Volkov, D. Ehberger *et al.*, "Polarized phonons carry angular momentum in ultrafast demagnetization," Nature **602**, 73–77 (2022).
[48]K. Neeraj, M. Pancaldi, V. Scalera *et al.*, "Magnetization switching in the inertial regime," Phys. Rev. B **105**, 054415 (2022).
[49]Y. Mi, K. Johnston, V. Shumakova *et al.*, "Active stabilization of terahertz waveforms radiated from a two-color air plasma," Photonics Res. **10**, 96–103 (2022).
[50]D. You, R. R. Jones, P. H. Bucksbaum, and D. R. Dykaar, "Generation of high-power sub-single-cycle 500-fs electromagnetic pulses," Opt. Lett. **18**, 290–292 (1993).
[51]S. Sederberg, F. Kong, and P. B. Corkum, "Tesla-scale terahertz magnetic impulses," Phys. Rev. X **10**, 011063 (2020).
[52]T. J. Davis, D. Janoschka, P. Dreher *et al.*, "Ultrafast vector imaging of plasmonic skyrmion dynamics with deep subwavelength resolution," Science **368**, eaba6415 (2020).
[53]Y. Dai, Z. Zhou, A. Ghosh *et al.*, "Plasmonic topological quasiparticle on the nanometre and femtosecond scales," Nature **588**, 616–619 (2020).
[54]A. Ghosh, S. Yang, Y. Dai *et al.*, "A topological lattice of plasmonic merons," Appl. Phys. Rev. **8**, 041413 (2021).
[55]Y. Dai, Z. Zhou, A. Ghosh *et al.*, "Ultrafast nanofemto photoemission electron microscopy of vectorial plasmonic fields," MRS Bull. **46**, 738–746 (2021).
[56]Y. Dai, Z. Zhou, A. Ghosh, K. Kapoor, M. Dąbrowski, A. Kubo, C.-B. Huang, and H. Petek, "Ultrafast microscopy of a twisted plasmonic spin skyrmion," Appl. Phys. Rev. **9**, 011420 (2022).
[57]J. Wätzel and J. Berakdar, "Centrifugal photovoltaic and photogalvanic effects driven by structured light," Sci. Rep. **6**, 21475 (2016).
[58]J. Wätzel, C. M. Granados-Castro, and J. Berakdar, "Magnetoelectric response of quantum structures driven by optical vector beams," Phys. Rev. B **99**, 085425 (2019).
[59]A. Lekosiotis, C. Brahms, F. Belli, T. F. Grigorova, and J. C. Travers, "Ultrafast circularly polarized pulses tunable from the vacuum to deep ultraviolet," Opt. Lett. **46**, 4057–4060 (2021).
[60]F. Reiter, U. Graf, M. Schultze *et al.*, "Generation of sub-3 fs pulses in the deep ultraviolet," Opt. Lett. **35**, 2248–2250 (2010).
[61]E. Goulielmakis, M. Schultze, M. Hofstetter *et al.*, "Single-cycle nonlinear optics," Science **320**, 1614–1617 (2008).
[62]B. E. Schmidt, A. D. Shiner, P. Lassonde *et al.*, "CEP stable 1.6 cycle pulses at 1.8 μm," Opt. Express **19**, 6858–6864 (2011).
[63]G. Andriukaitis, T. Balciunas, S. Altsauskas *et al.*, "90 GW peak power few-cycle mid-infrared pulses from an optical parametric amplifier," Opt. Lett. **36**, 2755–2757 (2011).
[64]A. D. Koulouklidis, C. Gollner, V. Shumakova *et al.*, "Observation of extremely efficient terahertz generation from mid-infrared two-color laser filaments," Nat. Commun. **11**, 292 (2020).
[65]A. de la Torre, D. M. Kennes, M. Claassen, S. Gerber, J. W. McIver, and M. A. Sentef, "Colloquium: Nonthermal pathways to ultrafast control in quantum materials," Rev. Mod. Phys. **93**, 041002 (2021).
[66]M. Reutzel, A. Li, Z. Wang, and H. Petek, "Coherent multidimensional photoelectron spectroscopy of ultrafast quasiparticle dressing by light," Nat. Commun. **11**, 2230 (2020).
[67]J. Güdde, M. Rohleder, T. Meier, S. W. Koch, and U. Höfer, "Time-resolved investigation of coherently controlled electric currents at a metal surface," Science **318**, 1287–1291 (2007).
[68]H. Petek, A. P. Heberle, W. Nessler, H. Nagano, S. Kubota, S. Matsunami, N. Moriya, and S. Ogawa, "Optical phase control of coherent electron dynamics in metals," Phys. Rev. Lett. **79**, 4649–4652 (1997).
[69]P. Dienstbier, T. Paschen, and P. Hommelhoff, "Two-color coherent control in photoemission from gold needle tips," J. Phys. B **54**, 134002 (2021).
[70]M. X. Na, A. K. Mills, F. Boschini *et al.*, "Direct determination of mode-projected electron-phonon coupling in the time domain," Science **366**, 1231–1236 (2019).
[71]P. Peng, Y. Mi, M. Lytova *et al.*, "Coherent control of ultrafast extreme ultraviolet transient absorption," Nat. Photonics **16**, 45–51 (2022).
[72]M. Hohenleutner, F. Langer, O. Schubert *et al.*, "Real-time observation of interfering crystal electrons in high-harmonic generation," Nature **523**, 572–575 (2015).
[73]T. L. Cocker, D. Peller, P. Yu, J. Repp, and R. Huber, "Tracking the ultrafast motion of a single molecule by femtosecond orbital imaging," Nature **539**, 263–267 (2016).